CRYSTAL GROWTH & DESIGN

Article

pubs.acs.org/crystal

# Role of Ethynyl-Derived Weak Hydrogen-Bond Interactions in the Supramolecular Structures of 1D, 2D, and 3D Coordination Polymers Containing 5-Ethynyl-1,3-benzenedicarboxylate

Jane V. Knichal, William J. Gee, Andrew D. Burrows,* Paul R. Raithby,* and Chick C. Wilson*

Department of Chemistry, University of Bath, Claverton Down, Bath BA2 7AY, United Kingdom

Supporting Information

**ABSTRACT:** The influence of weak hydrogen bonds on the crystal packing of a series of heavy and transition metal coordination polymers synthesized using the ligand 5-ethynyl-1,3-benzenedicarboxylic acid ($H_2$**ebdc**) has been evaluated. Five coordination polymers were prepared and crystallographically characterized. These comprise two 1D chains, [Pb(**ebdc**)$(DMSO)_2$] (**1**) and [Pb(**ebdc**)(DMF)] (**2**), two 2D nets, $[Cu_3$(**ebdc**)$(H_2O)_{1.5}(MeOH)_{0.5}]\cdot 6H_2O$ (**3**) and $[Pb_2$(**ebdc**$)_2(DMF)_4]\cdot H_2O$ (**4**), and a single 3D framework, $[HNEt_3][Zn_3(\mu_3\text{-}OH)(\mu_2\text{-}H_2O)$(**ebdc**$)_3(MeOH)_{0.67}(H_2O)_{0.33}]\cdot MeOH\cdot 1.33H_2O$ (**5**). The crystal structure of the free acid ligand form, $H_2$**ebdc**$\cdot H_2O$, is also reported. Within the lead(II) coordination structures, ethynyl-derived C−H···O interactions are consistently found to provide the dominant influence over the crystal packing, as determined by solid-state structural analysis in combination with vibrational spectroscopy. The influence of weak hydrogen-bonding effects on the crystal packing of the transition metal coordination polymers that contain lattice water and methanol molecules was found to be far less prominent, which is interpreted in terms of the greater prevalence of strong hydrogen-bond donors and acceptors forming O−H···O interactions within these crystalline lattices.

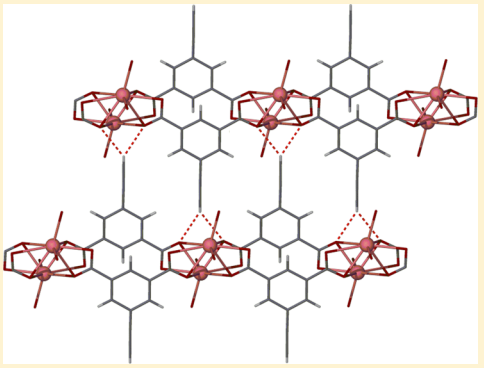

## INTRODUCTION

The design of crystalline architectures employing an understanding of the intermolecular interactions available to molecular subunits is the basis for crystal engineering, a key field straddling solid-state molecular assembly and structural analysis, whose importance lies in its capability for allowing control of crystal properties and functions as well as its structure.[1,2] Much progress has been made using simple systems composed of covalent[3] or strong hydrogen bonds;[4] however, control over weak hydrogen-bonding interactions remains one of the most challenging areas of crystal engineering.[5] A weak hydrogen bond can broadly be defined as an electrostatic interaction formed by a hydrogen atom between two structural moieties of moderate to low electronegativity, of which C−H···X (X = O/N) interactions are a key example. The study of these interactions began with the discovery of increased polarization of haloforms with ketones, pyridines, and ethers.[6] This observation was linked by spectroscopic interpretations to hydrogen bonding, to account for large bathochromic shifts observed in the infrared (IR) spectra of such species.[7] While assignment of these interactions by crystallography were initially resisted in the wake of strong criticisms by Donohue[8] toward a study by Sutor,[9,10] in recent years, advancements in the field of crystallography and in computational power have demonstrated and confirmed the fundamental importance of these interactions to supramolecular self-assembly. Such interactions can vary in strength from near equivalence to van der Waals interactions[11] to being stronger than weak covalent bonds and rivalling traditional hydrogen bonds.[12] In many crystalline networks, weak hydrogen bonds can be thought of as having a steering effect that may preferentially favor a single solid form, for example, a particular polymorph with solid-state packing governed largely by stronger intermolecular interactions but which is supplemented by contributions from weak directional C−H···X interactions.[5] However, there are known instances wherein weak hydrogen bonds are formed preferentially over interactions involving available strong donors or acceptors.[13,14] This preference for weak hydrogen bonds ensures that structural predetermination will fail if predictive methods rely solely on the traditional hierarchy of bonding strengths. Thus, the crystal engineer must view the sum of all interactions, both weak and strong, in order to predict the intermolecular architecture and crystal packing of a material, as opposed to focusing only on the strongest few interactions. This requirement necessitates an in-depth study of weak hydrogen-bonding interactions in order to understand fully, and integrate better, these stabilizing forces into the wider tenets of crystal engineering.

The ethynyl group is an attractive functionality for the study of weak hydrogen bonding owing to its highly activated nature

**Received:** October 15, 2014
**Revised:** November 28, 2014
**Published:** December 2, 2014

   dx.doi.org/10.1021/cg501535b | *Cryst. Growth Des.* 2015, 15, 465−474

Table 1. Crystallographic Data for $H_2$ebdc and Coordination Polymers 1−5[a]

| | $H_2$ebdc·$H_2O$ | 1 | 2 | 3 | 4 | 5 |
|---|---|---|---|---|---|---|
| formula | $C_{10}H_8O_5$ | $C_{14}H_{16}O_6PbS_2$ | $C_{78}H_{54}N_6O_{30}Pb_6$ | $C_{61}H_{27}Cu_6O_{41}$ | $C_{58}H_{58}N_6O_{23}Pb_4$ | $C_{75.34}H_{71.02}N_2O_{34.66}Zn_6$ |
| formula weight | 208.16 | 551.58 | 2798.41 | 1797.07 | 2035.86 | 1951.22 |
| crystal system | triclinic | monoclinic | triclinic | monoclinic | tetragonal | monoclinic |
| space group | $P\bar{1}$ | $P2_1/n$ | $P\bar{1}$ | $I2/a$ | $P\bar{4}2_1c$ | $P2_1/c$ |
| $a$, Å | 3.6787(2) | 9.9878(5) | 10.1240(4) | 22.3063(4) | 11.6687(1) | 11.1171(3) |
| $b$, Å | 9.5290(6) | 17.8249(6) | 15.0418(5) | 18.2460(3) | 11.6687(1) | 14.9906(6) |
| $c$, Å | 13.7468(10) | 10.5770(4) | 15.0480(6) | 21.5618(4) | 25.1110(4) | 24.3281(8) |
| $\alpha$, deg | 91.611(5) | 90 | 73.172(3) | 90 | 90 | 90 |
| $\beta$, deg | 92.252(6) | 115.088(6) | 75.343(3) | 95.649(2) | 90 | 93.217(3) |
| $\gamma$, deg | 100.278(5) | 90 | 71.172(3) | 90 | 90 | 90 |
| $V$, Å | 473.49(6) | 1705.39(15) | 2043.59(13) | 8733.0(3) | 3419.08(7) | 4047.9(2) |
| $Z$ | 2 | 4 | 1 | 4 | 2 | 2 |
| $\rho_{calc}$, g/cm$^3$ | 1.460 | 2.148 | 2.274 | 1.367 | 1.978 | 1.601 |
| reflns measured | 6367 | 14 229 | 20 695 | 50 261 | 20 310 | 33 693 |
| unique reflns | 2289 | 4512 | 8941 | 10 996 | 4246 | 11 001 |
| no. obsd ($I > 2\sigma(I)$) | 1248 | 3066 | 6637 | 8481 | 3822 | 7037 |
| $R_1$ | 0.0624 | 0.0600 | 0.0596 | 0.0570 | 0.0313 | 0.0964 |
| $wR_2$ | 0.1396 | 0.1121 | 0.1166 | 0.1726 | 0.0671 | 0.2168 |
| GOF | 0.901 | 1.016 | 1.072 | 1.054 | 1.098 | 1.154 |
| temp, K | 150(1) | 150(2) | 150(1) | 150(1) | 150(1) | 150(1) |

[a]Selected bond lengths and angles for the coordination polymers **1**−**5** are available as Supporting Information.

and acidity.[15] It is also ideally suited to spectroscopic study in the solid state, owing to its prominent C(sp)−H vibrational band in terms of intensity and unique location. Indeed examples of the C(sp)−H···O hydrogen bond match moderately strong O−H···O hydrogen bonds geometrically and, in terms of trends, spectroscopically.[16] This finding has been supported by studies comparing the hydrogen-bonding potential energy curves of weak acidic hydrogen bonds to O−H···O bonds that showed matching distributions.[5,17] The ethynyl group can act cooperatively as a hydrogen-bond acceptor via the alkyne $\pi$ system, as well as containing a donor site from the C(sp)−H hydrogen, enhancing hydrogen-bond strength by mutual polarization.[5] Similar cooperatively is one factor that provides strength to traditional O−H···O−H···O−H hydrogen-bonded chains.

Evaluation of the weak C−H···O hydrogen bonding observed for coordination polymers in this study has been achieved by single-crystal diffraction studies in order to obtain accurate interatomic donor−acceptor distances ($D$) and angular properties ($\theta$) of the hydrogen donor approaching the acceptor atom, in conjunction with analysis of C(sp)−H hydrogen bands by vibrational spectroscopy and changes to thermal vibrations observed in the crystal structure[18] that result from hydrogen-bond interactions. The coordination networks studied allow a comparison of networks containing hard acids (copper(II) and zinc(II)) that exhibit well-defined coordination geometries with those of lead(II), a softer metal center that permits a more flexible coordination environment. It is hoped that increasing the coordination flexibility about the metal center will translate into optimal ligand orientations for ethynyl-based weak hydrogen bonding, which will allow the targeted synthesis of materials containing such interactions, aiding in their study.

This work forms part of ongoing programs developing functional metal−ligand systems, including MOFs,[19] coordination polymers,[20] and organometallic clusters.[21−23]

## EXPERIMENTAL METHODS

**Caution:** ***Metal perchlorates are potentially explosive! Only a small amount of material should be prepared and handled with great care.*** Starting materials and solvents were purchased from commercial sources and used without further purification, with the exception of $H_2$**ebdc**, for which single crystals were grown by slow diffusion of water into a concentrated methanol solution. X-ray diffraction data for $H_2$**ebdc** and compounds **1**−**5** were collected on an Agilent Gemini A-Ultra diffractometer[24] at the University of Bath using Mo K$\alpha$ radiation, with the crystal being cooled to 150 K by an Agilent Cryojet.[25] Powder X-ray diffraction patterns (PXRDs) were recorded on a Bruker AXS D8 Advance diffractometer with Cu K$\alpha$ radiation of wavelength 1.5406 Å at 298 K. Samples were placed on a flat plate and measured with a 2$\theta$ range of 3−60°. Simulated X-ray powder patterns were generated from single-crystal data that were imported into PowderCell. Infrared spectra were recorded on a PerkinElmer Spectrum 100 spectrometer equipped with an ATR sampling accessory. Abbreviations for IR bands are s, strong; m, medium; w, weak. Elemental analyses (C, H, N) were performed on a CE-440 elemental analyzer (Exeter Analytical).

**Synthesis of [Pb(ebdc)(DMSO)$_2$] (1).** Colorless prismatic crystals of **1** were obtained by solvothermal synthesis using $Pb(OAc)_2{\cdot}3H_2O$ (0.08 g, 0.21 mmol) and 5-ethynyl-1,3-benzenedicarboxylic acid ($H_2$**ebdc**) (0.04 g, 0.21 mmol) dissolved in DMSO (5 mL) in a sealed vial and placed in a 100 °C oven for 4 days. Bulk purity was determined by PXRD. Anal. Calcd (%) for $C_{14}H_{16}O_6PbS_2$: C, 30.48; H, 2.92. Found: C, 30.36; H, 2.83. FTIR: $\bar{\nu}$ = 3221 (m), 3001 (w), 2913 (w), 1723 (w), 1661 (w), 1608 (m), 1592 (w), 1548 (s), 1414 (w), 1356 (s), 1122 (w), 1099 (m), 1016 (s), 993 (s), 953 (s), 790 (m), 777 (s), 743 (w), 722 (s) cm$^{-1}$.

**Synthesis of [Pb(ebdc)(DMF)] (2).** Colorless prismatic crystals of lead chain **2** were obtained by solvothermal synthesis of $Pb(OAc)_2{\cdot}3H_2O$ (0.08 g, 0.21 mmol) and $H_2$**ebdc** (0.04 g, 0.21 mmol) dissolved in DMF (5 mL) in a sealed vial and placed in a 140 °C oven for 2 days. Bulk purity was determined by PXRD. Anal. Calcd (%) for $C_{78}H_{54}N_6O_{30}Pb_6$: C, 33.48; H, 1.95; N, 3.00. Found: C, 33.42; H, 2.04; N, 3.11. FTIR: $\bar{\nu}$ = 3247 (m), 2931 (w), 1644 (s), 1593 (m), 1517 (s), 1424 (s), 1412 (s), 1352 (s), 1233 (m), 1101 (m), 918 (m), 789 (m), 773 (s), 717 (s), 663 (s) cm$^{-1}$.

**Synthesis of [Cu$_3$(ebdc)(H$_2$O)$_{1.5}$(MeOH)$_{0.5}$]·6H$_2$O (3).** Copper network **3** was crystallized by layered diffusion of $Cu(ClO_4)_2{\cdot}6H_2O$ (0.04 g, 0.11 mmol) in $H_2O$ (1 mL) and $H_2$**ebdc** (0.02 g, 0.11 mmol)


dx.doi.org/10.1021/cg501535b | Cryst. Growth Des. 2015, 15, 465−474

in MeOH (1 mL) containing a drop of $NEt_3$ after several days. The layers were allowed to slowly diffuse over several days through a 1:1 ($H_2O$/MeOH) buffer layer (2 mL). Turquoise block crystals were obtained. Bulk purity was determined by PXRD. Anal. Calcd (%) for $C_{61}H_{27}Cu_6O_{41}$: C, 40.77; H, 1.51. Found: C, 40.89; H, 1.55. FTIR: $\bar{\nu}$ = 3283 (w), 1627 (m), 1579 (w), 1437 (m), 1412 (w), 1371 (s), 1307 (w), 1239 (w), 1113 (w), 916 (w), 771 (s), 731 (s) $cm^{-1}$.

**Synthesis of $[Pb_2(ebdc)_2(DMF)_4]\cdot H_2O$ (4).** Colorless prismatic crystals of lead network **4** were obtained by solvothermal synthesis using $Pb(OAc)_2\cdot 3H_2O$ (0.08 g, 0.21 mmol) and $H_2$**ebdc** (0.04 g, 0.21 mmol) dissolved in DMF (5 mL) in a sealed vial and placed in a 100 °C oven for 4 days. Bulk purity was determined by PXRD. Anal. Calcd (%) for $C_{55}H_{53}N_5O_{24}Pb_4$ (substitution of one DMF molecule for two molecules of $H_2O$): C, 32.23; H, 2.81; N, 3.55. Found: C, 32.15; H, 2.61; N, 3.40. FTIR: $\bar{\nu}$ = 3246 (m), 2931 (w), 1645(s), 1593 (m), 1518 (s), 1425 (s), 1382 (w), 1352 (s), 1233 (m), 1102 (s), 984 (w), 918 (m), 789 (w), 773 (m), 718 (s) $cm^{-1}$.

**Synthesis of $[HNEt_3][Zn_3(\mu_3\text{-}OH)(\mu_2\text{-}H_2O)(ebdc)_3(MeOH)_{0.67}(H_2O)_{0.33}]\cdot MeOH\cdot 1.33H_2O$ (5).** Zinc network **5** was obtained by slow layering of $Zn(ClO_4)_2\cdot 6H_2O$ (0.04 g, 0.11 mmol) in $H_2O$ and $H_2$**ebdc** (0.02 g, 0.11 mmol) in MeOH with trace amounts of $NEt_3$ for several days at room temperature in a sealed vial. The layers were allowed to slowly diffuse through a 1:1 ($H_2O$/MeOH) buffer layer. Yellow plate crystals were obtained. Bulk purity was determined by PXRD. Anal. Calcd (%) for $C_{75.34}H_{71}N_2O_{34.66}Zn_6$: C, 46.37; H, 3.67; N, 1.44. Despite repeated attempts on multiple batches of crystalline material, satisfactory elemental analysis data could not be obtained. FTIR: $\bar{\nu}$ = 3270 (w), 1612 (m), 1575 (m), 1432 (m), 1403 (w), 1359 (s), 1236 (w), 1108 (w), 1008 (w), 912 (m), 771 (s), 723 (s) $cm^{-1}$.

## RESULTS AND DISCUSSION

**Analysis of $H_2$ebdc·$H_2O$.** The ligand used in this study, 5-ethynyl-1,3-benzenedicarboxylic acid ($H_2$**ebdc**), has not been previously crystallographically analyzed. It possesses two carboxylic acid functional groups to allow coordination of metal nodes upon deprotonation and an ethynyl group to promote weak hydrogen-bonding interactions. Nontarget interactions that are allowed by this ligand include $\pi-\pi$ stacking derived from the central aromatic ring as well as strong hydrogen bonding from either the carboxylic acid or carboxylate functionality.

Crystalline $H_2$**ebdc**·$H_2O$ was obtained by layering a concentrated methanol solution over a water layer and was found to adopt the triclinic space group $P\bar{1}$ (Table 1). The asymmetric unit contains both $H_2$**ebdc** and a single hydrogen-bonded molecule of lattice water. A 1D hydrogen-bond network propagates along nodes of four $H_2$**ebdc** molecules and two water molecules, composed of three rings of interactions, two outer rings designated $R_3^3(10)$, and an inner ring designated $R_4^2(8)$ according to Etter's notation[26] (Figure 1). Hydrogen-bond distances of 2.586(3) Å, O(3)···O(5); 2.594(3) Å, O(2′)···O(4); 2.823(3) Å, O(5)···O(1′); and 2.843(3) Å, O(5)···O(1′) were observed.

The ethynyl group is located in the vicinity of O(2′) of a symmetry-generated molecule ($-x$ − 1, 2 − $y$, 1 − $z$) of $H_2$**ebdc** (Figure 2); however, any hydrogen bonding is likely to be extremely weak based on the observed distance $D$ of 3.337(3) Å and approach angle $\theta$ of 147°. Instead, the ethynyl group appears to order the structure solely by interdigitation. Consequently, the IR vibration spectrum of the free ethynyl C−H stretching band for $H_2$**ebdc** was assigned as 3301 $cm^{-1}$, providing a reference point for any bathochromic shifts that occur with hydrogen-bond formation in the coordination polymers of this ligand reported below. Furthermore, a decrease in the $C_{terminal}/C_{inner}$ thermal parameter ratio for the terminal ethynyl group may serve as a qualitative measure of hydrogen bonding; hence, the nonbonded value for $H_2$**ebdc** (C(10)/C(9)) was determined to be 1.37, which is within the range found for known nonbonded terminal ethynyl groups, albeit near the lower limit.[18]

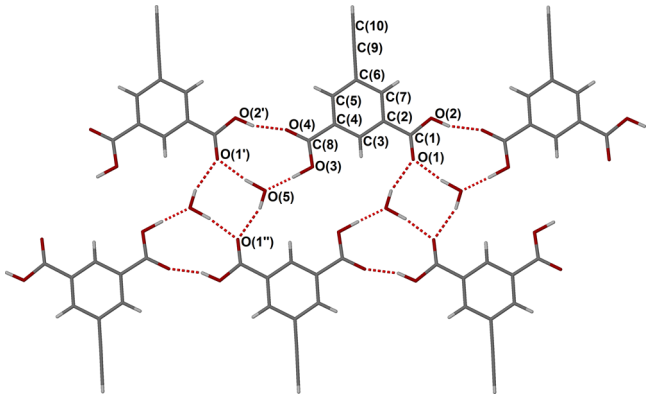


**Figure 1.** Crystalline $H_2$**ebdc**·$H_2O$ showing a network of hydrogen-bonding interactions.

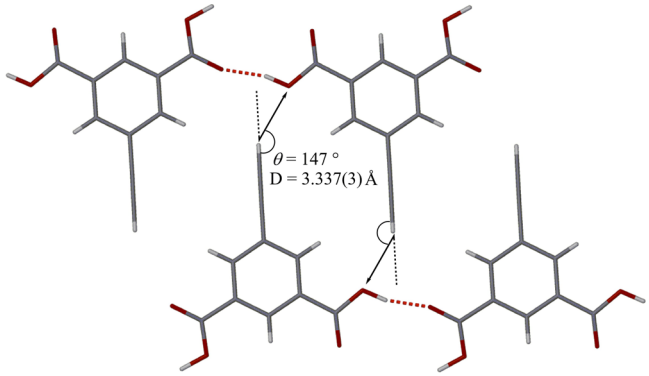


**Figure 2.** Crystalline aggregation of $H_2$**ebdc** molecules in the structure of $H_2$**ebdc**·$H_2O$ showing the nearest contact between the ethynyl group and O(2′).

Five coordination polymers, comprising two 1D chains, [Pb(**ebdc**)$(DMSO)_2$] (**1**) and [Pb(**ebdc**)(DMF)] (**2**), two 2D nets, $[Cu_3(\mathbf{ebdc})(H_2O)_{1.5}(MeOH)_{0.5}]\cdot 6H_2O$ (**3**) and $[Pb_2(\mathbf{ebdc})_2(DMF)_4]\cdot H_2O$ (**4**), and a single 3D framework, $[HNEt_3][Zn_3(\mu_3\text{-}OH)(\mu_2\text{-}H_2O)(\mathbf{ebdc})_3(MeOH)_{0.67}(H_2O)_{0.33}]\cdot MeOH\cdot 1.33H_2O$ (**5**), were synthesized from $H_2$**ebdc**, with the crystal data obtained in this study summarized in Table 1. Tables of selected bond lengths and angles for each of the coordination polymers **1**−**5** are available as Supporting Information.

**Synthetic Overview.** The equimolar reaction of $H_2$**ebdc** with hydrated divalent metal salts gives rise to coordination polymers consistent with the known affinity of meta-substituted aromatic carboxylic acids for such species.[27−29] The hierarchy of molecular interactions is ultimately governed by covalent metal−carboxylate interactions involving the deprotonated **ebdc** ligand, which yield the primary structure. Inclusion of the ligand guarantees the presence of the ethynyl group, ensuring the possibility of weak hydrogen bonds influencing the secondary molecular packing. However, a range of polar protic and aprotic solvents were used during the synthesis of **1**−**5** (Scheme 1), and no effort was made to exclude water from the synthesis or crystallization processes; hence, competition with strong solvent-mediated hydrogen bonding has been allowed


dx.doi.org/10.1021/cg501535b | Cryst. Growth Des. 2015, 15, 465−474

**Scheme 1. Synthesis of Coordination Polymers 1−5**[a]

$Pb(OAc)_2{\cdot}3H_2O + H_2$**ebdc** $\xrightarrow{a}$ [Pb(**ebdc**)$(DMSO)_2$] (**1**)
$Pb(OAc)_2{\cdot}3H_2O + H_2$**ebdc** $\xrightarrow{b}$ [Pb(**ebdc**)(DMF)] (**2**)
$Cu(OAc)_2{\cdot}2H_2O + H_2$**ebdc** + $NEt_3 \xrightarrow{c}$ $[Cu_3$(**ebdc**)$(H_2O)_{1.5}(MeOH)_{0.5}]{\cdot}6H_2O$ (**3**)
$Pb(OAc)_2{\cdot}3H_2O + H_2$**ebdc** $\xrightarrow{d}$ $[Pb_2$(**ebdc**)$_2(DMF)_4]{\cdot}H_2O$ (**4**)
$Zn(OAc)_2{\cdot}2H_2O + H_2$**ebdc** + $NEt_3 \xrightarrow{e}$
$[HNEt_3][Zn_3(\mu_3\text{-}OH)(\mu_2\text{-}H_2O)$(**ebdc**$)_3(MeOH)_{0.67}(H_2O)_{0.33}]{\cdot}MeOH{\cdot}1.33H_2O$ (**5**)

[a]Reagents and conditions: (a) DMSO, 100 °C; (b) DMF, 140 °C; (c) MeOH/$H_2O$ (1:1), $NEt_3$, rt; (d) DMF, 100 °C; (e) MeOH/$H_2O$ (1:1), $NEt_3$, rt.

and may dominate crystal packing, as observed in the solid-state structure of $H_2$**ebdc**·$H_2O$. For Pb systems, the nature of the product obtained is dependent on the solvent used and the temperature of the reaction.

**Lead Chain 1.** The asymmetric unit of **1** was found to contain a single lead(II) center ligated by an **ebdc** ligand and two molecules of DMSO, one of which is disordered over two positions. The structure propagates such that the lead(II) is eight-coordinate, with each **ebdc** ligand coordinating to three lead(II) atoms and with each carboxylate chelating in a $\mu$-($\mu O$:$\kappa O'$) manner (Figure 3). This includes two secondary

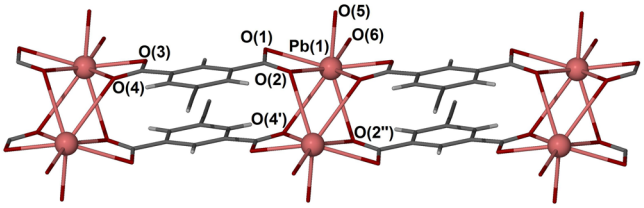


**Figure 3.** Molecular structure of 1D chain [Pb(**ebdc**)$(DMSO)_2$] **1**. Only the oxygen atoms for each molecule of DMSO (O5 and O6) have been shown for clarity.

interactions within the limits of van der Waals interactions for lead and oxygen (2.75 < 3.30 Å), Pb(1)−O(4′) (1 − $x$, −$y$, 2 − $z$), 3.248(7) Å; Pb(1)−O(2″) (2 − $x$, −$y$, 2 − $z$), 3.079(7) Å. The long contacts pair together simple chains of [Pb(**ebdc**)-$(DMSO)_2$].

Packing of the 1D chains results from bifurcated donor C−H···O hydrogen bonding derived from the ethynyl group and links to O(2′) and O(4′) of two carboxylate groups (Figure 4). Distances for C(9)···O(2′) of 3.286(8) Å and C(9)···O(4′) of 3.213(9) Å were observed, and the angle of the ethynyl group is 170° relative to the plane of the carboxylate oxygen atoms, favoring the observed hydrogen-bonding interactions. A significant bathochromic shift of 80 $cm^{-1}$ was observed in the IR spectrum, and the ratio of thermal vibration for C(9) and C(8) decreased to 1.33, suggesting inhibition as a result of hydrogen bonding. These interactions occur on either side of the 1D chain and collectively yield a 2D hydrogen-bonded network that packs in a herringbone arrangement (Figure S1, Supporting Information).

**Lead 2D Net 2.** Lead network **2** was formed by solvothermal synthesis in DMF at 140 °C and yields a 1D tape motif that crystallizes in the triclinic space group $P\bar{1}$. The asymmetric unit contains three unique lead(II) atoms that are ligated by three **ebdc** ligands and three coordinated molecules of DMF, two of which are disordered over two positions (Figure S2, Supporting Information). These propagate by symmetry to give repeating hexagonal rings of lead(II) atoms that are fused by bridging **ebdc** ligands (Figure 5). Pairs of

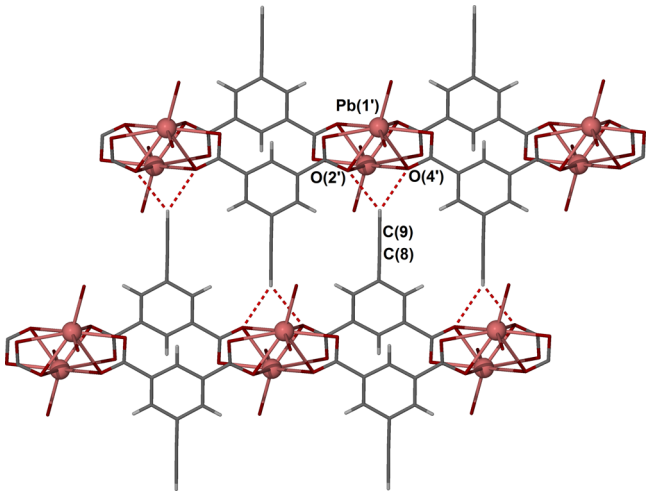


**Figure 4.** Bifurcated C−H···O hydrogen bonding observed between chains of **1**: $D$ = C(9)···O(2′), 3.286(8) Å; C(9)···O(4′), 3.213(9) Å. Each ethynyl group additionally participates in interdigitation and is maximally displaced from those present in the neighboring chain.

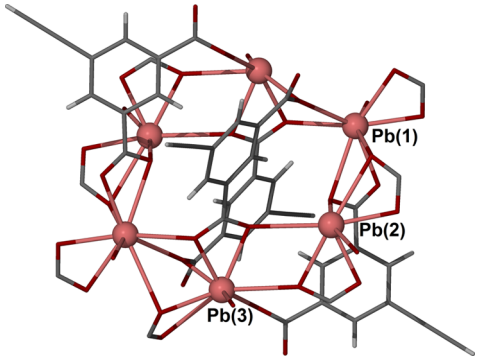


**Figure 5.** A single hexagonal array of $Pb^{2+}$ atoms present within the tape structure of **2**. Only the oxygen atom of the single DMF molecules coordinating each metal has been shown for clarity.

**ebdc** ligands direct ethynyl groups above and below the tape, and a single ligand bridges the remaining orthogonal faces, ensuring that the periphery of the tape is shrouded by weak hydrogen donors (Figure 6). Bridging modes exhibited by the six carboxylate groups include $\mu$-($\mu O$:$\kappa O'$), $\mu_3$-($\mu O$:$\mu O'$), and $\mu_4$-($\mu_3 O$:$\mu O'$), which result in one nine-coordinate and two seven-coordinate lead(II) centers. There are three unique ethynyl groups that have the potential to form hydrogen-bond interactions (Figure 7). Bifurcated ethynyl C−H···O hydrogen

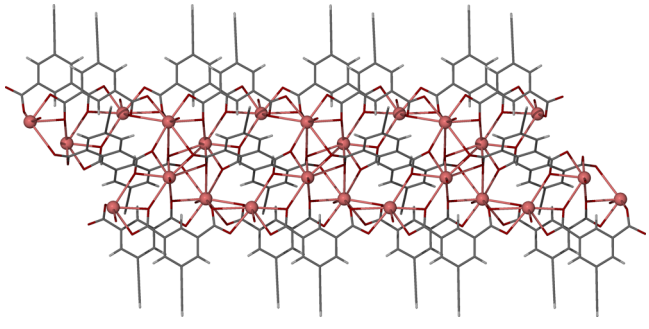

**Figure 6.** Extended 1D tape structure of **2** showing an array of ethynyl-based hydrogen donors.


dx.doi.org/10.1021/cg501535b | Cryst. Growth Des. 2015, 15, 465−474

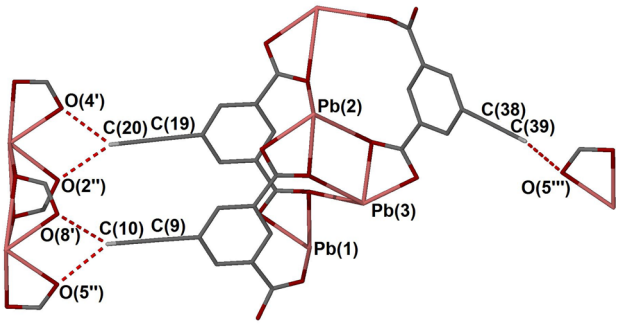


**Figure 7.** Three unique ethynyl groups in **2** with potential for weak hydrogen bonding. Symmetry codes: O(4′) and O(8′) $(1 - x, 1 - y, 1 - z)$, O(2″) and O(5″) $(-x, 1 - y, 1 - z)$, and O(5‴) $(1 + x, y, z - 1)$.

bonding analogous to that of **1** was observed in two instances in the structure of **2**, with paired distances of C(10)···O(5″), 3.279(10) Å; C(10)···O(8′), 3.308(11) Å; and C(20)···O(2″), 3.282(10) Å; C(20)···O(4′), 3.194(10) Å. The former hydrogen-bond interaction aligns with an angle of 164°, the latter, to 179°, with the plane of the carboxylate oxygen atoms. The final ethynyl group is directly oriented toward the oxygen atom of a carboxylate group (C(39)···O(5‴)) with an angle of 170°; however, the distance is long at 3.562(17) Å. No other significant interactions form between the 1D chains, suggesting that weak hydrogen-bonding interactions are solely responsible for the crystal packing in **2**. Despite the presence of three distinct ethynyl groups within the asymmetric unit of **2**, only a single band with a prominent shoulder directed toward lower wavenumbers was observed in the IR spectrum. The dominant vibration exhibited a bathochromic shift of 56 $cm^{-1}$ relative to the nonbonded reference and has been assigned to the bifurcated pair of terminal alkynes, owing to its intensity relative to the shoulder band that is likely a result of its proximity to an oxygen acceptor. Furthermore, the shoulder exhibits greater red-shifting, which has been observed for directly aligned, as opposed to bifurcated, C−H···O interactions (vide infra). The ratios of $C_{terminal}/C_{inner}$ thermal vibrations for the bifurcated hydrogen-bond interactions are 1.31 and 1.47, which suggests that the former, C(20)···O(4′), holds more hydrogen-bonding character, likely owing to its more favorable orientation angle of 179°. The final ethynyl group has a very high $C_{terminal}/C_{inner}$ thermal parameter ratio of 1.73; however, this may be a result of its proximity to a neighboring disordered DMF site. In such instances, infrared analysis should be considered the most reliable indicator for weak hydrogen-bond identification.[5]

**Copper 2D Net 3.** The 2D copper network **3** crystallizes in the monoclinic *I*2/*a* space group and exhibits formation of the characteristic copper paddlewheel motif. The asymmetric unit contains two copper(II) atoms bridged by a carboxylate group from three **ebdc** ligands, one of which coordinates the third copper(II) atom via the second carboxylate group. The apical positions of the paddlewheel are occupied by coordinated water molecules, one of which exhibits 50:50 substitutional site disorder with a methanol molecule. Five molecules of water are located in the lattice, four of which are disordered over more than one position. The extended molecular structure forms a $t_1\{6,3\}$ 2D net, whereby the paddlewheels link to assemble a Kagomé lattice (Figure 8). Each 2D sheet is offset relative to the sheets above and below. In this manner, the network is

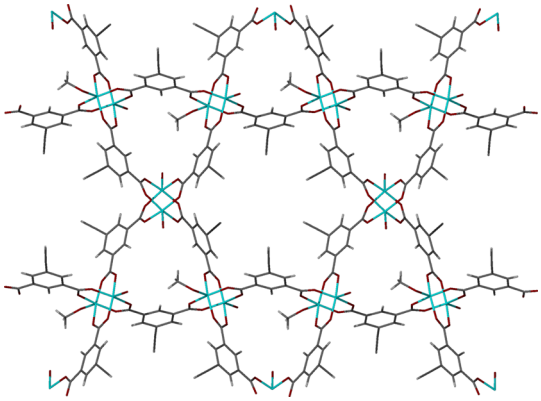

**Figure 8.** 2D Kagomé lattice arrangement observed for **3**.

similar to that formed by copper(II) with other 1,3-benzenedicarboxylates (bdc), such as 5-nitro-1,3-bdc and 5-(methylsulfanylmethyl)-1,3-bdc.[30]

Of the three unique **ebdc** ligands, two are oriented toward the carboxylate groups of the layer above, and one is oriented toward a lattice water molecule below (Figure 9). Competing

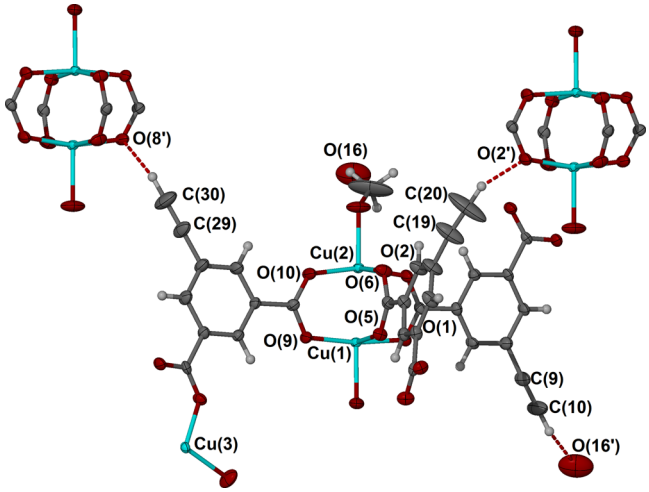


**Figure 9.** Closest ethynyl contacts for the three unique ligands observed in **3**. Thermal ellipsoids are shown with 50% probability. The methanol molecule coordinating Cu(2) exhibits substitutional disorder with a coordinated water molecule and O(16).

interactions include $\pi-\pi$ stacking that directly link the layers and a network of strong hydrogen bonding. The former is a parallel offset interaction with an intercentroid distance of 3.67 Å (closest $\pi-\pi$ contact, 3.60 Å), linking this ligand with its symmetry equivalent in a second net. Interaction between the two nets is strengthened by a hydrogen-bonding array between the apical solvent molecules of the paddlewheel and lattice water molecules (Figure 10). While the quality of the crystallographic data was insufficient to locate the individual hydrogen atoms using the electron density map, interoxygen distances give strong evidence for the presence of a strong hydrogen-bonding network, exemplified by distances of 2.687(5) Å for O(15)···O(17) and 2.760(5) Å for O(17)···O(13′) $({}^3/_2 - x, {}^3/_2 - y, {}^1/_2 - z)$.

The closest internetwork ethynyl contacts are 3.217(4) Å for C(20)···O(2) and 3.198(4) Å for C(30)···O(8). The final ethynyl group is directed toward a lattice water molecule with a distance of 3.249(5) Å for C(10)···O(16). Despite the relatively


dx.doi.org/10.1021/cg501535b | *Cryst. Growth Des.* 2015, 15, 465−474

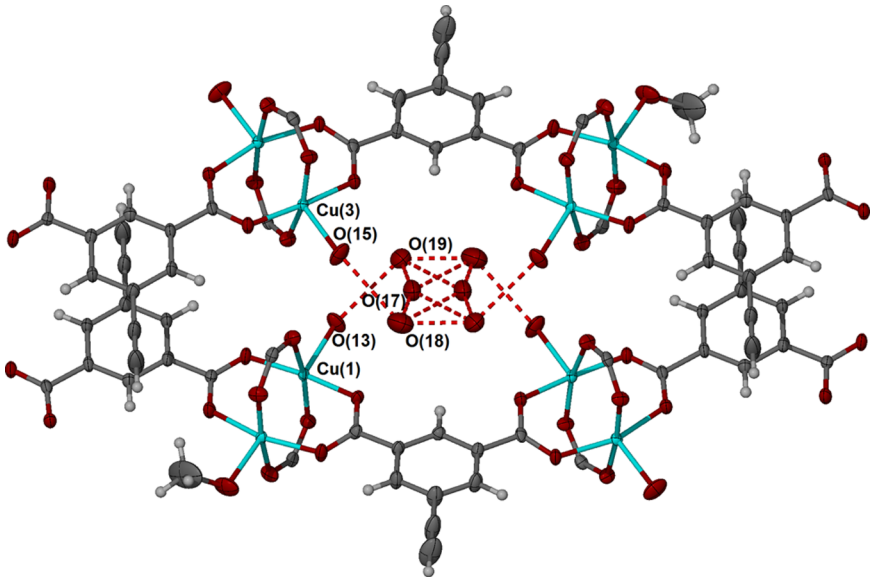


**Figure 10.** Hydrogen-bonding interactions involving lattice water molecules that partition the 2D sheets in **3**. Thermal ellipsoids are shown with 50% probability.

close proximity of the ethynyl donor groups to the oxygen acceptors, the angles are not conducive of a significant hydrogen-bonding interaction, ranging from 143 to 152°.

The IR spectrum of **3** shows that the band intensity for the ethynyl C−H stretching vibrations centered at 3287 $cm^{-1}$ has decreased and broadened considerably, with each effect being characteristic of the absence of significant hydrogen bonding.[31] Greater thermal vibration was observed between the terminal and inner sp carbons of the alkyne, with $C_{terminal}/C_{inner}$ ratios of 1.66, 1.74, and 1.40, which provides further evidence for a lack of hydrogen-bonding interactions. In this instance, the crystal packing appears to be determined by interactions other than those of weak hydrogen bonding (i.e., strong hydrogen bonding and/or $\pi-\pi$ stacking described earlier).

**Lead 2D Net 4.** Crystals of 2D lead network $[Pb_2(\mathbf{ebdc})_2(DMF)_4]\cdot H_2O$ (**4**) were obtained by heating a mixture of $H_2$**ebdc** and hydrated lead acetate in DMF at 100 °C. The network crystallizes in the tetragonal space group $P\bar{4}2_1c$, and the asymmetric unit contains a single lead(II) atom ligated via the carboxylate of a single **ebdc** ligand, two DMF molecules, of which one is disordered over a special position, and a single lattice water molecule with half occupancy that is also located on a special position (Figure S3, Supporting Information). The lead(II) atoms are eight-coordinate and aggregate to form a $Pb_4O_4$ cubane motif (Figure 11) in which each cubane node linked to four others by pairs of bridging **ebdc** ligands to give an extended (4,4) 2D net (Figure 12). The two carboxylate groups of **ebdc** have different coordination modes, whereby one carboxylate chelates a single lead(II) atom in a $\kappa O{:}\kappa O'$ manner, and the second carboxylate forms the corner of the cubane cluster, thereby coordinating three lead atoms in a $\mu_3$-($\mu_3 O{:}\kappa O'$) fashion. Ethynyl-derived weak hydrogen bonds constitute the only interactions linking the 2D sheets, in which the ethynyl groups of bridging **ebdc** ligands coordinating to carboxylate groups located above or below the net in an alternating fashion. The C(10)···O(1′) hydrogen bond to the carboxylate group of a symmetry generated cluster ($^3/_2 - x$, $y - {}^1/_2 - y$, $^3/_2 - z$) has a distance of 3.152(5) Å, with a favorable angle for bonding of 171° (Figure 13).

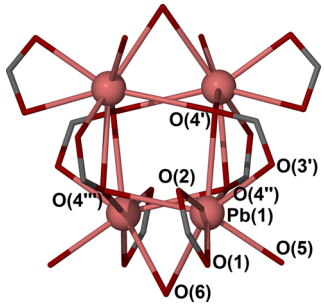


**Figure 11.** $Pb_4O_4$ cubane motif that acts as a secondary building unit in **4**. Only the carboxylate groups of **ebdc** and the oxygen contacts of coordinated DMF molecules have been shown for clarity.

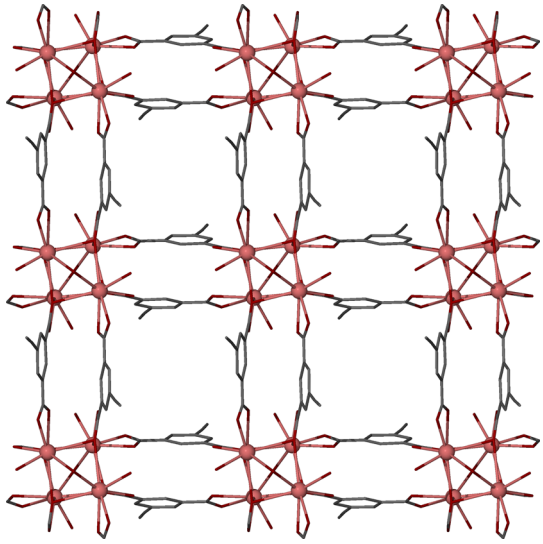

**Figure 12.** Extended (4,4) 2D network present in **4**.

Network **4** exhibits the largest bathochromic shift of compounds **1**−**5**, wherein the terminal C−H stretch shifts 89 $cm^{-1}$ to 3212 $cm^{-1}$. Similarly, the lowest ratio of thermal vibration between the terminal and adjacent carbon atoms of


dx.doi.org/10.1021/cg501535b | *Cryst. Growth Des.* 2015, 15, 465−474

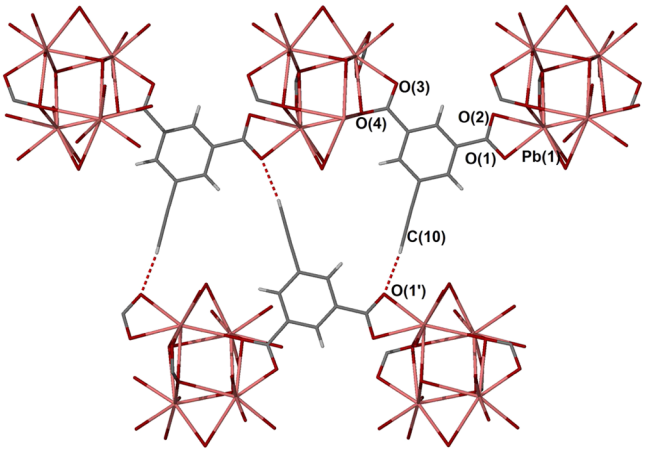


**Figure 13.** Weak hydrogen-bonding interactions between C(10) and O(1′) ($^3/_2 - x, y - {}^1/_2 - y, {}^3/_2 - z$), $D$ = 3.152(5) Å, $\theta$ = 171°, link 2D sheets of **4** in the solid state.

the alkyne, of 1.31, was observed for **ebdc** in **4**. This observation can be explained by the alkyne group aligning to a single oxygen site (O(1′), $D$ = 3.152(5) Å, $\theta$ = 171°), unlike in cases **1** and **2**, where the interaction is spread over two oxygen receptors, allowing more vibration between the two sites.

**Zinc 3D Net 5.** The final coordination polymer, $[HNEt_3][Zn_3(\mu_3{-}OH)(\mu_2\text{-}H_2O)(\mathbf{ebdc})_3(MeOH)_{0.67}(H_2O)_{0.33}]\cdot MeOH\cdot 1.33H_2O$ (**5**) consists of three zinc(II) atoms arrayed in a triangular cluster about a central $\mu_3$-OH group, which are ligated by three **ebdc** ligands and two aqua ligands, of which one is substitutionally disordered with a molecule of methanol. The anionic structure is charge-balanced in the lattice by a triethylammonium cation that contains one ethyl arm disordered over two positions. A molecule of methanol and three molecules of water, each with partial occupancy, complete the asymmetric unit. Two of the zinc(II) atoms are four-coordinate and exhibit tetrahedral coordination geometry. The final zinc(II) atom is six-coordinate with octahedral coordination geometry. The coordinated water molecule and a symmetry equivalent bridge between two $Zn_3(OH)^{5+}$ clusters, generating a hexanuclear motif that is held together by OH···O hydrogen bonds involving the hydroxy and aqua ligands (Figure 14). Of the six carboxylate groups, four coordinate to the cluster in a $\kappa$-*COO* manner, with the nonbonding oxygen atom hydrogen bonding to the $\mu_3$-OH group, O(1)···O(9) ($D$ = 2.815(8) Å), O(1)···O(13) ($D$ = 2.981(8) Å) or with the bridging $\mu_2$-$H_2O$ group, O(2)···O(12) ($D$ = 2.624(7) Å), O(2)···O(8) ($D$ = 2.726(7) Å). These interactions are designated as S(6) and S(8) graph set motifs, respectively. The remaining two carboxylate groups bridge between two zinc centers in a $\mu$-($\kappa O$:$\kappa O'$) manner. Each solvent molecule present in the lattice also participates in hydrogen bonding, but it proved to be difficult to assign hydrogen positions unambiguously (for this reason, only a single methanol molecule has been shown in Figure 14). The lattice methanol molecule forms hydrogen bonds to the carboxylate and coordinated methanol, O(19)···O(9) ($D$ = 2.684(9) Å), O(15)···O(19) ($D$ = 2.705(7) Å), which can be designated as $R_3^2(8)$. Pairs of **ebdc** ligands further stabilize the cluster core by $\pi$–$\pi$ stacking parallel to the bridging water molecules (Figure 15). The participating ligands are symmetry-equivalent and give a parallel offset interaction with an intercentroid

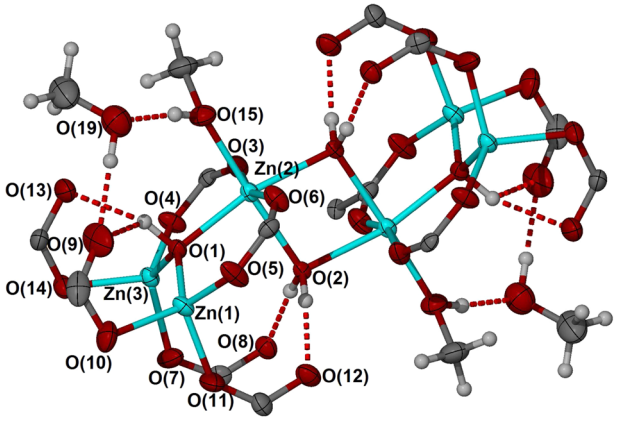


**Figure 14.** Strong hydrogen-bonding interactions present around the fused $[Zn_6(\mu_3\text{-}OH)_2(\mu_2\text{-}H_2O)_2]^{10+}$ cluster core of **5**. Only the carboxylate groups from ligated **ebdc** have been shown, along with one solvent methanol molecule; the counterions and remaining lattice solvents have been omitted for clarity. Thermal ellipsoids are shown with 50% probability.

distance of 3.59 Å (closest $\pi$–$\pi$ contact, 3.38 Å). The 3D network propagates by bridging **ebdc** ligands of fused $[Zn_6(\mu_3\text{-}OH)_2(\mu_2\text{-}H_2O)_2]^{10+}$ centers, forming 1D channels that contain solvent and counterions (Figure 16). Analogous hexanuclear zinc(II) secondary building units have been observed in a limited number of instances.[32,33]

There are three unique ethynyl groups within the 3D network of **5**. Two of these groups align in a manner suggestive of C–H···$\pi$ hydrogen-bond interaction, with one acting solely as a donor and the other solely as an acceptor (Figure 17). Such T-shaped dimers have been calculated to impart stabilization energies on the order of 1.0 to 2.0 kcal/mol.[34] The average C(20)–H···$\pi$ distance is 2.74 Å, which is equivalent to the mean distance (2.72 Å) observed in a study of such terminal alkyne interactions.[5] The final ethynyl group is directed toward the carboxylate group of an adjacent ligand with a C(30)···O(8) distance of 3.453(7) Å and an offset angle of 153° (Figure 18).

As in the case of copper network **3**, the band intensity for the ethynyl C–H stretching vibration is both decreased and broadened; however, three unique bands were observable at 3301, 3271, and 3252 $cm^{-1}$ that can be assigned to the three ethynyl groups. The non-hydrogen-bonding ethynyl ligand in **5** matches the frequency of the non-hydrogen-bonding reference of $H_2$**ebdc**, at 3301 $cm^{-1}$. The band at 3271 $cm^{-1}$ is red-shifted by 30 $cm^{-1}$, which is characteristic of C–H···$\pi$ bonding,[4] and also possesses the strongest intensity, which likely reflects the optimal T-shaped geometry of the interaction shown in Figure 17. The final band at 3252 $cm^{-1}$ has a red-shift of 49 $cm^{-1}$ and likely corresponds to the ethynyl C–H···O bond in Figure 18, with its diminished intensity likely a result of poor alignment with the carboxylate.

**Packing Influence of ebdc.** This study has identified several lead(II) networks, **1**, **2**, and **4**, which exhibit ethynyl-based weak hydrogen-bonding interactions that directly influence crystal packing. Two factors appear to favor C(sp)–H···O interactions within these structures, the first being the flexible coordination polyhedra imparted by the lead(II) atoms in conjunction with O-donor ligands. This allows the **ebdc** ligands to adopt a wide range of coordination modes and thus possess more freedom to achieve optimal hydrogen-bonding geometry. The second factor, in part, may relate to the choice


dx.doi.org/10.1021/cg501535b | *Cryst. Growth Des.* 2015, 15, 465–474

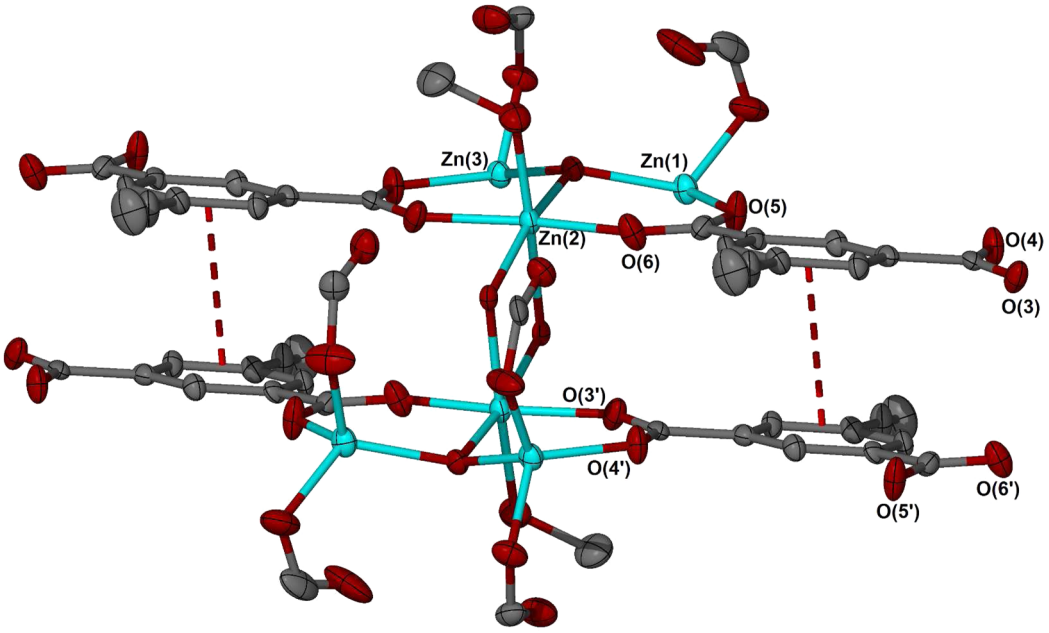


**Figure 15.** Pairs of **ebdc** $\pi-\pi$ stacking interactions located either side of the $[Zn_6(\mu_3\text{-}OH)_2(\mu_2\text{-}H_2O)_2]^{10+}$ cluster core further stabilize this motif. Thermal ellipsoids are shown with 50% probability.

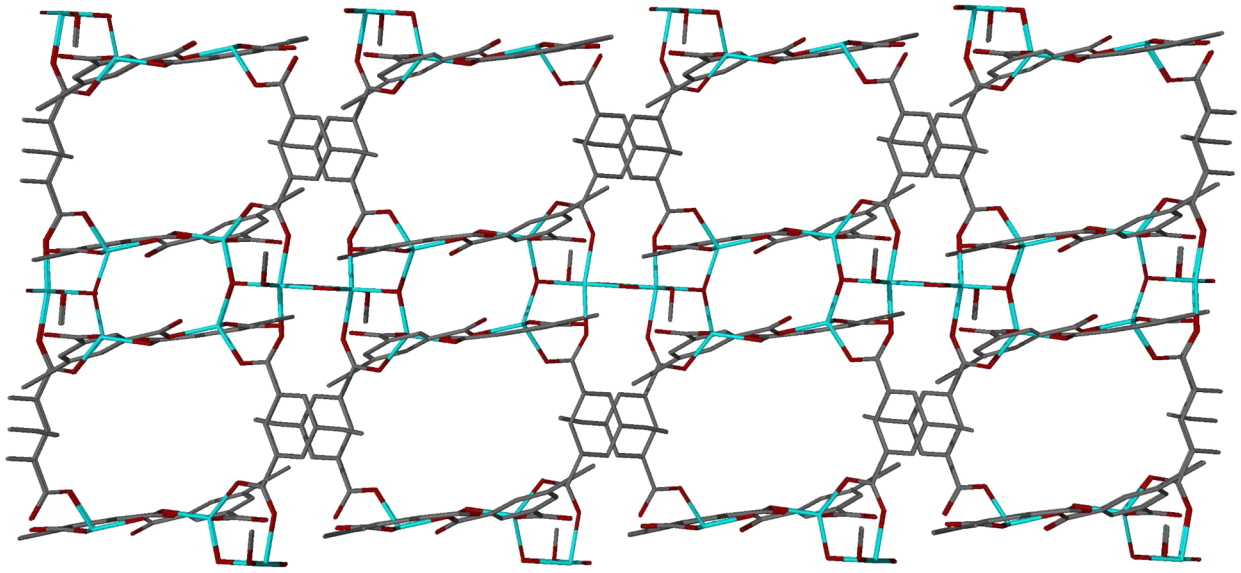

**Figure 16.** One-dimensional solvated channels propagating through structure **5**. The lattice triethylammonium, methanol, and water molecules have been omitted to highlight the channels.

of polar aprotic solvents during synthesis of the lead(II) coordination polymers. This solvent choice may have resulted in the number of hydrogen-bond acceptors far exceeding the number of donors, which would maximize the likelihood of the ethynyl groups of **ebdc** achieving a high degree of utilization.

By contrast, the two transition metal structures, **3** and **5**, are both found to contain extensive hydrogen-bonding arrays as well as $\pi-\pi$ stacking interactions, both of which are lacking in the lead(II) structures. Only minor **ebdc**-based weak hydrogen-bonding interactions were observed by IR spectroscopy, suggesting that the crystal packing, and thus self-assembly process, for these structures was not governed by weak hydrogen-bonding interactions to any large extent. While methanol was found to participate in these hydrogen-bonding nets, in most cases, it was observed to be substitutionally disordered with water molecules; water was also available in the wet solvents used during synthesis of the lead(II) structures. This suggests that solvent choice is not the main reason for a lack of weak hydrogen-bonding interactions. Instead, it is likely that the more rigid coordination environment provided by the transition metals promotes the inclusion of more coordinated solvent, which in turn increases the availability of strong hydrogen donors. The apical positions of the copper paddlewheel motif, which are typically coordinated by aqua ligands,[35] demonstrates this effect. Similarly, the high Lewis acidity of zinc(II) promotes formation of hydroxo species and, in turn, cluster formation, which also likely favors strong, as opposed to weak, hydrogen bonding through the inclusion of more strong hydrogen donors into the crystalline structure. This provides the rationale for the contrasting behavior of lead


dx.doi.org/10.1021/cg501535b | *Cryst. Growth Des.* 2015, 15, 465−474

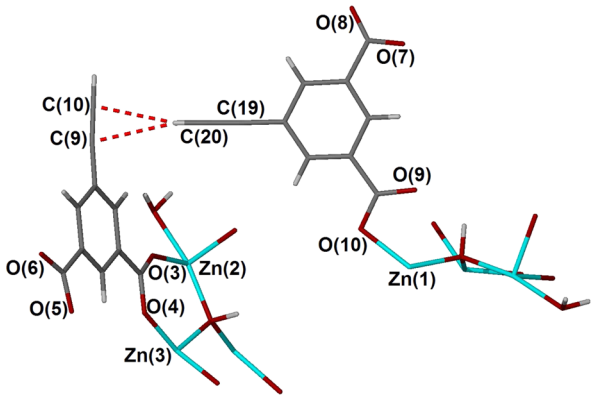


**Figure 17.** A weak C−H···$\pi$ hydrogen-bond interaction between C(20) and the ethynyl $\pi$ region, average $D$ = 2.74 Å, in **5**.

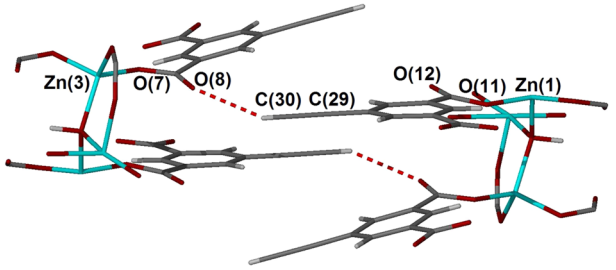


**Figure 18.** The offset weak hydrogen-bonding interaction between C(30) and O(8′), $D$ = 3.453(7) Å, $\theta$ = 153.2°, links the 3D network of **5** in the solid state.

and transition metal complexes with respect to the influence of hydrogen bonding in their solid-state assembly.

While gaining control over weak hydrogen-bond interactions during the self-assembly of coordination polymers remains a distant goal at the present time, this study has identified lead(II) and its corresponding coordination polymers as interesting species for study using ligands containing weak hydrogen-bond donors, in which the resulting weak hydrogen bonds are influential in forming the solid state-structures. This work will be expanded to include a range of other heavy metals ligated by **ebdc** as well as varying the weak hydrogen-bond donor on similar diacids in combination with lead(II) to extend the scope of these findings.

## CONCLUSIONS

Of the five coordination polymers studied, three examples have been identified where weak hydrogen bonding derived from the ethynyl groups of the dicarboxylate ligand **ebdc** dominates the crystal packing and thus molecular self-assembly, namely, [Pb(**ebdc**)(DMSO)$_2$] (**1**), [Pb(**ebdc**)(DMF)] (**2**), and [Pb$_2$(**ebdc**)$_2$(DMF)$_4$]·H$_2$O (**4**). These lead(II) networks have proven to be valuable systems for the study of weak C(sp)−H···O hydrogen-bonding interactions, both by single-crystal X-ray crystallography and IR spectroscopy. Two transition metal networks were also investigated, [Cu$_3$(**ebdc**)-(H$_2$O)$_{1.5}$(MeOH)$_{0.5}$]·6H$_2$O (**3**) and [HNEt$_3$][Zn$_3$($\mu_3$-OH)-($\mu_2$-H$_2$O)(**ebdc**)$_3$(MeOH)$_{0.67}$(H$_2$O)$_{0.33}$]·MeOH·1.33H$_2$O (**5**); however, in these instances, strong hydrogen-bonding interactions predominated. Future work will establish if other heavy metals ligated by **ebdc** exhibit similar behavior to that of lead(II) and the possibility of varying the ethynyl group for other weak hydrogen-bond donors that may control the architecture in lead(II) networks.

## ASSOCIATED CONTENT

### Supporting Information

Packing motif of **1** (Figure S1), asymmetric units of **2** (Figure S2) and **4** (Figure S3), hydrogen-bonding tables for H$_2$**ebdc** and **5**, selected bond lengths and angles, and PXRD spectra for networks **1**−**5**. This material is available free of charge via the Internet at http://pubs.acs.org. CCDC 1025919−1025924 contain the supplementary crystallographic data for this article. These data can be obtained free of charge from The Cambridge Crystallographic Data Centre via http://www.ccdc.cam.ac.uk/Community/Requestastructure/Pages/DataRequest.aspx?.

## AUTHOR INFORMATION

### Corresponding Authors

*(A.D.B.) E-mail: a.d.burrows@bath.ac.uk.
*(P.R.R.) E-mail: p.r.raithby@bath.ac.uk.
*(C.C.W.) E-mail: c.c.wilson@bath.ac.uk.

### Author Contributions

The manuscript was written through contributions of all authors. All authors have given approval to the final version of the manuscript.

### Notes

The authors declare no competing financial interest.

## ACKNOWLEDGMENTS

We are grateful to the EPSRC for financial support of the project (EP/K004956/1) and the University of Bath for a studentship to J.V.K.

## ABBREVIATIONS

H$_2$**ebdc**, 5-ethynyl-1,3-benzenedicarboxylic acid; bdc, 1,3-benzenedicarboxylate; IR, infrared; CCDC, Cambridge Crystallographic Data Centre; 1D, one dimensional; 2D, two dimensional; 3D, three dimensional; PXRDs, powder X-ray diffraction patterns

## REFERENCES

(1) Moulton, B.; Zaworotko, M. J. *Chem. Rev.* **2001**, *101*, 1629−1658.
(2) Biradha, K.; Su, C.-Y.; Vittal, J. J. *Cryst. Growth Des.* **2011**, *11*, 875−886.
(3) Blake, A. J.; Champness, N. R.; Hubberstey, P.; Li, W.-S.; Withersby, M. A.; Schröder, M. *Coord. Chem. Rev.* **1999**, *183*, 117−138.
(4) Desiraju, G. R. *Acc. Chem. Res.* **2002**, *35*, 565−573.
(5) Desiraju, G. R.; Steiner, T. *The Weak Hydrogen Bond in Structural Chemistry and Biology*; Oxford University Press: New York, 1999.
(6) Glasstone, S. *Trans. Faraday Soc.* **1937**, 200−214.
(7) Gordy, W. *J. Chem. Phys.* **1939**, *7*, 163−166.
(8) Donohue, J. Selected Topics in Hydrogen Bonding. In *Structural Chemistry and Molecular Biology*; Rich, A., Davidson, N., Eds.; Freeman: San Francisco, CA, 1968; pp 443−465.
(9) Sutor, D. J. *Nature* **1962**, *195*, 68−69.
(10) Sutor, D. J. *J. Chem. Soc.* **1963**, 1105−1110.
(11) Howard, J. A. K.; Hoy, V. J.; O'Hagan, D.; Smith, G. T. *Tetrahedron* **1996**, *52*, 12661−12622.
(12) Gronert, S. *J. Am. Chem. Soc.* **1993**, *115*, 10258−10266.
(13) Atwood, J. L.; Harnada, F.; Robinson, K. D.; Orr, G. W.; Vincent, R. L. *Nature* **1991**, *349*, 683−684.
(14) Desiraju, G. R.; Sharma, C. V. K. M. *J. Chem. Soc., Chem. Comm.* **1991**, 1239−1241.

(15) Allerhand, A.; Schleyer, P. v. R. *J. Am. Chem. Soc.* **1963**, *85*, 1715−1723.
(16) Kariuki, B. M.; Harris, K. D. M.; Philip, D.; Robinson, J. M. A. *J. Am. Chem. Soc.* **1997**, *119*, 12679−12689.
(17) Steiner, T. *J. Chem. Soc., Chem. Commun.* **1995**, 95−96.
(18) Steiner, T. *J. Chem. Soc., Chem. Commun.* **1994**, 101−102.
(19) Burrows, A. D.; Frost, C. G.; Mahon, M. F.; Richardson, C. *Angew. Chem., Int. Ed.* **2008**, *47*, 8482−8486.
(20) Knichal, J. V.; Gee, W. J.; Burrows, A. D.; Raithby, P. R.; Teat, S. J.; Wilson, C. C. *Chem. Commun.* **2014**, *50*, 14436−14439.
(21) Warren, M. R.; Easun, T. L.; Brayshaw, S. K.; Deeth, R. J.; George, M. W.; Johnson, A. L.; Schiffers, S.; Teat, S. J.; Warren, A. J.; Warren, J. E.; Wilson, C. C.; Woodall, C. H.; Raithby, P. R. *Chem.—Eur. J.* **2014**, *20*, 5468−5477.
(22) Hatcher, L. E.; Christensen, J.; Hamilton, M. L.; Trincao, J.; Allan, D. R.; Warren, M. R.; Clarke, I. P.; Towrie, M.; Fuertes, S.; Wilson, C. C.; Woodall, C. H.; Raithby, P. R. *Chem.—Eur. J.* **2014**, *20*, 3128−3134.
(23) Hatcher, L. E.; Warren, M. R.; Allan, D. R.; Brayshaw, S. K.; Johnson, A. L.; Fuertes, S.; Schiffers, S.; Stevenson, A. J.; Teat, S. J.; Woodall, C. H.; Raithby, P. R. *Angew. Chem., Int. Ed.* **2011**, *50*, 8371−8374.
(24) *Agilent Gemini A-Ultra Diffractometer*. http://www.chem.agilent.com/en-US/products-services/Instruments-Systems/X-Ray-Crystallography/Gemini/Pages/default.aspx.
(25) *Agilent CryojetXL*. http://www.chem.agilent.com/en-US/products-services/Instruments-Systems/X-Ray-Crystallography/Cryojet5/Pages/default.aspx.
(26) Bernstein, J.; Davis, R. E.; Shimoni, L.; Chang, N.-L. *Angew. Chem., Int. Ed. Engl.* **1995**, *34*, 1555−1573.
(27) Yang, E.-C.; Li, J.; Ding, B.; Liang, Q.-Q.; Wang, X.-G.; Zhao, X.-J. *CrystEngComm* **2008**, *10*, 158−161.
(28) Zhang, L.; Qin, Y.-Y.; Li, Z.-J.; Lin, Q.-P.; Cheng, J.-K.; Zhang, J.; Yao, Y.-G. *Inorg. Chem.* **2008**, *47*, 8286−8293.
(29) Zhang, Z.; Zhou, Y.-L.; He, H.-Y. *Acta Crystallogr., Sect. E: Struct. Rep. Online* **2006**, *62*, m2591−m2593.
(30) Burrows, A. D.; Frost, C. G.; Mahon, M. F.; Winsper, W.; Richardson, C.; Attfeld, J. P.; Rodgers, J. A. *Dalton Trans.* **2008**, 6788−6795.
(31) Lutz, B. T. G.; Jacob, J.; van der Maas, J. H. *Vib. Spectrosc.* **1996**, *12*, 197−206.
(32) Fang, Q.-R.; Zhu, G.-S.; Xue, M.; Zhang, Q.-L.; Sun, J.-Y.; Guo, X.-D.; Qui, S.-L.; Xu, S.-T.; Wang, P. *Chem.—Eur. J.* **2006**, *12*, 3754−3758.
(33) Zhang, J.-P.; Lin, Y.-Y.; Weng, Y.-Q.; Chen, X.-M. *Inorg. Chim. Acta* **2006**, *359*, 3666−3670.
(34) Scheiner, S. *Hydrogen Bonding: A Theoretical Perspective*; Oxford University Press: New York, 1997.
(35) Eddaoudi, M.; Moler, D. B.; Li, H. L.; Chen, B. L.; Reineke, T. M.; O'Keeffe, M.; Yaghi, O. M. *Acc. Chem. Res.* **2001**, *34*, 319−330.